

# Excitation Transfer Engineering in Ce-Doped Oxide Crystalline Scintillators by Codoping with Alkali-Earth Ions

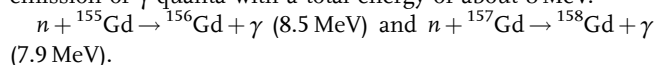
Etiennette Auffray, Ramūnas Augulis, Andrei Fedorov, Georgy Dosovitskiy, Larisa Grigorjeva, Vidmantas Gulbinas, Merry Koschan, Marco Lucchini, Charles Melcher, Saulius Nargelas, Gintautas Tamulaitis, Augustas Vaitkevičius, Aleksejs Zolotarjovs, and Mikhail Korzhik\*

Time-resolved spectroscopic study of the photoluminescence response to femtosecond pulse excitation and free carrier absorption at different wavelengths, thermally stimulated luminescence measurements and investigation of differential absorption are applied to amend the available data on excitation transfer in GAGG:Ce scintillators, and an electronic energy-level diagram in this single crystal is suggested to explain the influence of codoping with divalent Mg on luminescence kinetics and light yield. The conclusions are generalized by comparison of the influence of aliovalent doping in garnets (GAGG:Ce) and oxyorthosilicates (LSO:Ce and YSO:Ce). In both cases, the codoping facilitates the energy transfer to radiative  $\text{Ce}^{3+}$  centers, while the light yield is increased in the LYSO:Ce system but reduced in GAGG:Ce.

## 1. Introduction

Aliovalent codoping has been recently demonstrated to be a productive approach to improve the scintillation properties of bulk Ce-doped scintillators with different host structures. Codoping of Ce-doped gadolinium gallium aluminum garnet  $\text{Gd}_3\text{Al}_2\text{Ga}_3\text{O}_{12}$  (GAGG) single crystals with the divalent cation  $\text{Mg}^{2+}$  is highly promising for applications of this scintillator in the new generation of PET (positron emission tomography) scanners.<sup>[1,2]</sup> This scintillator is a product of purposeful engineering of the band gap and the energy position of the activator levels in the gap.<sup>[3,4]</sup> The crystal exhibits a high light yield of up to  $\approx 70\,000$  phot/MeV,<sup>[5]</sup> has luminescence decay time shorter than

100 ns, and its emission band peaks at  $\approx 520$  nm which perfectly matches the sensitivity spectrum of conventional Silicon Photomultipliers (SiPMs). Thus, the crystal might compete with  $\text{Lu}_2\text{SiO}_5\text{:Ce}$  (LSO:Ce) and  $(\text{Lu}_{1-x}\text{Y}_x)_2\text{SiO}_5\text{:Ce}$  (LYSO:Ce) in Time-of-Flight Positron Emission Tomography (TOF-PET) applications. Moreover, GAGG:Ce might become the scintillator of choice in high-resolution  $\gamma$ -radiation spectrometry and compete with the halide scintillators recently developed for this purpose.<sup>[6–8]</sup> Finally, natural gadolinium is a mixture of six stable isotopes,  $^{154}\text{Gd}$  (2.18%),  $^{155}\text{Gd}$  (14.8%),  $^{156}\text{Gd}$  (20.5%),  $^{157}\text{Gd}$  (15.7%),  $^{158}\text{Gd}$  (24.8%), and  $^{160}\text{Gd}$  (21.9%), two of which,  $^{155}\text{Gd}$  and  $^{157}\text{Gd}$ , have the highest neutron capture cross section among all known stable isotopes, 61 000 and 254 000 barns, respectively. The capture of neutrons is accompanied by the emission of  $\gamma$ -quanta with a total energy of about 8 MeV:



This energy release, as well as individual  $\gamma$ -quanta, can be detected by the same crystal in which the interaction takes place.

However, the outstanding characteristics of GAGG:Ce detectors are accompanied by certain shortcomings, hindering extensive application of the material in radiation detection. Particularly, the material exhibits strong phosphorescence, both under photoexcitation and excitation by ionizing radiation. It has

Dr. E. Auffray, Dr. M. Lucchini  
CERN  
1211 Geneva, Switzerland

Dr. R. Augulis, Dr. V. Gulbinas  
Center for Physical Sciences and Technology  
Savanorių av. 231, LT-02300 Vilnius, Lithuania

Dr. M. Koschan, Dr. C. Melcher  
University of Tennessee  
Knoxville, TN 37966, USA

Dr. G. Dosovitskiy  
National Research Center “Kurchatov Institute”  
Kurchatova 1, 123098 Moscow, Russia

Dr. L. Grigorjeva, Dr. A. Zolotarjovs  
Institute of Solid State Physics  
University of Latvia  
LV-1063 Riga, Latvia

Dr. S. Nargelas, A. Vaitkevičius, Dr. G. Tamulaitis  
Vilnius University  
Universiteto str. 3, LT-1513 Vilnius, Lithuania

Dr. M. Korzhik, Dr. A. Fedorov  
Research Institute for Nuclear Problems  
Bobruiskaya str. 11, 220030 Minsk, Belarus  
E-mail: mikhail.korzhik@cern.ch

DOI: 10.1002/pssa.201700798

been demonstrated that the phosphorescence might be diminished in the crystal and ceramics by codoping with Mg.<sup>[9,10]</sup>

Unfortunately, the codoping of GGAG:Ce by Mg results in a lower scintillation light yield (LY) at room temperature (RT), contrary to the codoping of LSO:Ce and LYSO:Ce by divalent Ca or Mg.<sup>[11,12]</sup> Recently, we demonstrated that the luminescence build up after short-pulse excitation becomes significantly faster, when GAGG:Ce crystal is codoped by Mg.<sup>[13]</sup> This observation of the shortening of the luminescence rise time is in line with the previous results on the coincidence time resolution, where substantial improvement of the response time in Mg-codoped GAGG:Ce crystals is observed at certain decrease of the light yield.<sup>[14]</sup> At a small energy release, using 511 keV gamma-rays from <sup>22</sup>Na source, the Coincidence Resolving Time (CTR) with full width at half maximum (FWHM) of 540 and 233 ps was measured in GAGG:Ce without and with Mg codoping, respectively. At high energy deposit, when high-energy charged particles have been used to excite the crystal, the Mg-codoped sample yielded a better single device time resolution of 30.5 ps sigma than that in Mg-free sample (36.2 ps sigma).<sup>[15]</sup> Finally, a significant improvement of GAGG:Ce,Mg light yield without changes in scintillation kinetics was observed, when the crystal temperature was progressively decreased down to  $-45^{\circ}\text{C}$ ,<sup>[16]</sup> what was not detected in the crystals doped solely with Ce.<sup>[17]</sup> These features make GAGG:Ce,Mg the scintillator of choice to operate with SiPM readout at reduced temperatures.

In spite of the spectacular progress in the improvement of the performance parameters of oxide crystalline scintillators with aliovalent co-doping, the mechanism of the improvement is still not fully understood.

This aliovalent doping, in which a trivalent ion is substituted by a divalent second group cation in the host matrix, results in the formation of anionic vacancies that compensate for the resulting charge. The formation of a hole-type defect including  $\text{Mg}^{2+}$  and  $\text{O}^{-}$  in close proximity is also quite probable.<sup>[18,19]</sup> Moreover, the codoping of Ce-activated crystals by divalent ions (even at the level of less than 1 at.%) causes oxidation of part of the  $\text{Ce}^{3+}$  ions to  $\text{Ce}^{4+}$ . Both cerium ions are involved in the scintillation process.<sup>[12,20,21]</sup> Codoping by  $\text{Ca}^{2+}$  or  $\text{Mg}^{2+}$  of oxide material crystallized at high temperature seems to introduce similar defects in the matrix due to similarity of the cation properties in the same host, though different dependence of the light yield on their concentration was observed in GAGG:Ce.<sup>[9]</sup>

It has also been demonstrated that codoping of  $\text{Y}_2\text{SiO}_5:\text{Ce}$ ,  $\text{LYSO}:\text{Ce}$ ,  $\text{LaBr}_3:\text{Ce}$ , and  $\text{CeBr}_3$  with divalent alkali-earth ions results in enhancement of scintillation light yield and improvement of the energy resolution of the detectors based on these materials.<sup>[12,22–25]</sup> Moreover, it was recently demonstrated that aliovalent co-doping by  $\text{Sr}^{2+}$  of the most widely used  $\text{NaI}(\text{Tl})$  scintillation crystals also improves their energy resolution.<sup>[26]</sup> This is an indication that the defect associated with the aliovalent codoping ( $\text{Mg}^{2+}$ ,  $\text{Ca}^{2+}$ ,  $\text{Sr}^{2+}$ ) is most likely a matrix host defect.

The cerium-doped lutetium oxyorthosilicate  $\text{Lu}_2\text{SiO}_5:\text{Ce}$  attracted our attention because of its extensive exploitation as scintillator in medical imaging devices. Codoping with divalent Ca results in substantial improvement of the scintillation properties of this crystal. Contrary to codoped GAGG:Ce, the light yield of aliovalently codoped LSO:Ce increases by 10–20%,

the scintillation decay becomes faster, and the phosphorescence is significantly suppressed.<sup>[12,27]</sup> These improvements are primarily caused by suppression of free carrier trapping by deep intrinsic traps. Nevertheless, the negative influence of Ca-codoping on formation of nonradiative recombination centers in LSO scintillators is still under study.

The current paper is aimed at revealing the mechanisms through which codoping of Ce-doped scintillation single crystals by divalent alkali-earth ions influences the luminescence and scintillation properties of these materials. Our study was primarily focused on the investigation of GAGG:Ce, which is a complicated system in view of the excitation transfer processes. The generalization of the mechanisms is based on comparison of the results obtained for GAGG:Ce and LSO:Ce, two scintillators with substantially different crystal fields, which turned out to be of importance for the competition of excitation transfer in crystals codoped with divalent ions. We exploited steady-state, quasi-steady-state and time-resolved photoluminescence spectroscopy and pump-and-probe techniques to study the dynamics of nonequilibrium carriers. The thermally stimulated emission technique was used to characterize the energy levels of the traps in the band gap. This study enabled us to construct simple schematic energy-level diagrams, which allow explaining the main routes of excitation transfer and the influence of the aliovalent codoping.

## 2. Experimental Section

The GAGG:Ce samples used in this study were grown by the Czochralski technique from iridium crucibles. The samples, in the shape of a  $3 \times 3 \times 5 \text{ mm}^3$  block, were cut from single crystal boules and subsequently polished. The key scintillation parameters of the samples are presented in **Table 1**.

Samples A1 and A2 were fabricated at the Institute of Physics, Czech Academy of Sciences. The crystals were grown in nominally identical conditions and with nominally the same cerium content of 0.5 at.%. In addition, A2 was codoped with magnesium at 0.1 at.%.

The set of GAGG:Ce samples labeled hereafter B1, B2, and B3 was prepared at the National Research Center “Kurchatov Institute” in Moscow, Russia, to investigate the influence of gallium evaporation on the crystal properties. These three samples, shaped as  $10 \times 10 \times 7 \text{ mm}^3$  blocks, were produced using sintered raw materials. Sample B1 was grown from the melt with stoichiometric composition. To compensate for gallium volatilization from the melt during growth, sample B2 was grown with excess  $\text{Ga}_2\text{O}_3$  added to the melt in the crucible. To further compensate for the volatilization of Ga and to inhibit the formation of oxygen vacancies more efficiently, codoping with tetravalent ions was exploited in sample B3 which was grown with 0.01 at.% of zirconium, in addition to the excess  $\text{Ga}_2\text{O}_3$  added as was done during the growth of sample B2.

Two types of oxyorthosilicates,  $\text{Lu}_2\text{SiO}_5$  and  $\text{Y}_2\text{SiO}_5$ , solely doped with Ce and codoped by Ca, both at 0.1 at.% in the melt, were labeled as L1 and L2 and measured to compare the change of the optical transmission spectra due to aliovalent codoping. The oxyorthosilicate boules, nominally 32 mm in diameter, were grown in inductively heated iridium crucibles by the Czochralski

**Table 1.** Scintillation parameters of GAGG samples under study.

Sample	Composition	Luminescence decay times ns (%)			Phosphorescence level, arb. u.	Light yield, ph/MeV
		Fast	Intermediate	Slow		
A1	Gd <sub>3</sub> Ga <sub>3</sub> Al <sub>2</sub> O <sub>12</sub> :Ce	52(23)	130(68)	230(9)	80	35 000
A2	Gd <sub>3</sub> Ga <sub>3</sub> Al <sub>2</sub> O <sub>12</sub> :Ce, Mg	56(40)	100(60)	–	–	27 000
B1	Gd <sub>3</sub> Ga <sub>3</sub> Al <sub>2</sub> O <sub>12</sub> :Ce	52(22)	150(67)	700(10)	100	26 000
B2	Gd <sub>3</sub> Ga <sub>3</sub> Al <sub>2</sub> O <sub>12</sub> :Ce excess Ga	51(10)	150(39)	2125(51)	335	31 000
B3	Gd <sub>3</sub> Ga <sub>3</sub> Al <sub>2</sub> O <sub>12</sub> :Ce excess Ga + 0.001 at.% Zr	63(27)	150(73)	–	700	21 000

method (see Ref. [23] for more detail). Uncodoped LSO:Ce crystal was studied in detail to reveal the energy transfer processes. The sample (L3) had dimensions 10 × 10 × 2 mm.

The scintillation kinetics was measured by the start-stop method. The luminescence decay of the samples was characterized using a fit by three exponential components. The light yield was measured by photomultiplier tube XP2020 calibrated using 1 inch CsI(Tl) reference crystal produced by Institute of Scintillation Materials (ISMA), Kharkov, Ukraine. The light yield provided in Table 1 was measured in the samples unannealed after crystal growth. These samples were used in all our experiments. The phosphorescence level was estimated at the background plateau measured simultaneously with the scintillation kinetics by the start-stop method. The scintillation properties of the samples were evaluated at room temperature.

In thermally stimulated luminescence (TSL) experiments, the thermal activation energy of the traps  $E_{TA}$  has been determined by the fractional glow method.<sup>[28]</sup> The TSL peaks were measured in the luminescence spectral range from 300 to 800 nm at the heating rate of 6 K min<sup>-1</sup>. The samples were activated for 30 min using an X-ray tube (30 kV, 15 mA) at 7 K.

The time-resolved photoluminescence (TRPL) study has been performed using a Hamamatsu streak camera. In synchroscan detection mode, the time resolution was limited by the instrumental response function with full-width at half maximum (FWHM) of 2.95 ps. To study the PL kinetics in the samples with long decay components, the camera could be operated only in a single sweep mode with considerably poorer time resolution. A femtosecond Yb:KGW oscillator (Light Conversion Ltd.) emitting at 1030 nm and producing 80 fs pulses at 76 MHz repetition rate was used as a primary excitation source. The third 3.64 eV (343 nm) and fourth 4.9 eV (254 nm) harmonics of the oscillator emission have been produced by a harmonics generator (HIRO, Light Conversion Ltd.) to ensure selective photoexcitation.

For GAGG:Ce crystals, the 3.6 eV (343 nm) emission resonantly excites Ce<sup>3+</sup> ions into the lowest excited energy level. Meanwhile, the photon energy of 4.9 eV (254 nm) corresponds to <sup>8</sup>S → <sup>6</sup>D<sub>7/2,9/2</sub> transition of Gd<sup>3+</sup> ions and also is sufficient to cause transitions to the long-wavelength wing of the band due to excitation into the third component of Ce<sup>3+</sup> electronic configuration 4f<sup>0</sup>5d<sup>1</sup>. For the LSO:Ce crystal, the 4.9 eV photons excite Ce<sup>3+</sup> ions into the third component as well.

The dynamics of free nonequilibrium carriers was investigated using free carrier absorption (FCA), which was measured using a pump and probe technique. The free carriers were

generated by short light pulses (200 fs) at 4.9 eV (254 nm). A part of the fundamental harmonic of the Yb:KGW laser described above was frequency-quadrupled using β-barium borate crystals and used for this purpose. The optical absorption of the samples was probed with a variable delay at different fixed wavelengths by using the output of a parametric generator in the infrared range 900–1700 nm (1.38–0.73 eV). The difference in the optical absorption with and without the pump (differential absorption, DA) was measured as a function of the delay between the pump and probe pulses. The DA in this spectral region is caused by the induced absorption, which is proportional to free carrier density.

### 3. Results

#### 3.1. Photoluminescence and Free Carrier Absorption in GAGG:Ce and GAGG:Ce,Mg

The codoping of GAGG:Ce with magnesium introduces a broad absorption band that peaks at 4.7 eV (265 nm), which is not observed in the crystal without codoping. The spectrum of the difference in absorption coefficients measured in samples A1 (GAGG:Ce) and A2 (GAGG:Ce, Mg) is presented in **Figure 1**. Both samples are grown in nominally the same conditions and

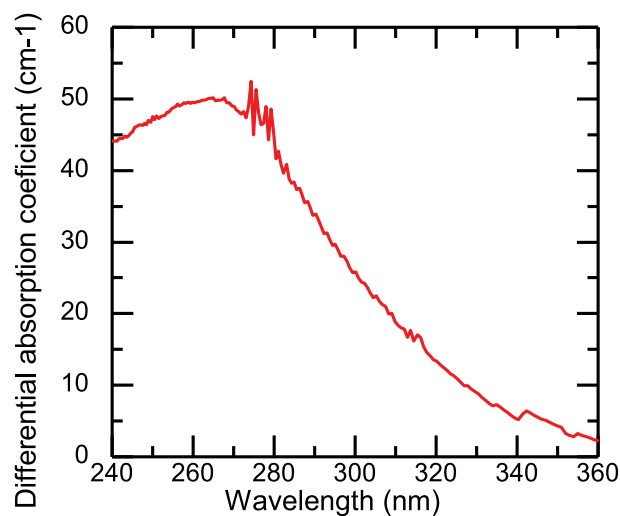


**Figure 1.** Spectrum of the difference in absorption coefficient of GAGG:Ce with and without magnesium codoping.

contain nominally the same concentration of  $\text{Ce}^{3+}$  ions. Thus, the change in absorption is caused by Mg codoping. However, no difference of the absorption intensity of the  $\text{Ce}^{3+}$  bands due to transfer to the first Stark component of  $\text{Ce}^{3+}$  electronic configuration  $4f^05d^1$  was observed in the samples. It indicates that conversion of  $\text{Ce}^{3+}$  ions into the  $\text{Ce}^{4+}$  state at such a low Mg concentration does not affect  $\text{Ce}^{3+}$  concentration significantly. This absorption band is most probably caused by charge transfer (CT) transition from the valence band to the defect stabilized by  $\text{Mg}^{2+}$ , one of which may be a  $\text{Ce}^{4+}$  ion.

The photoluminescence response of GAGG:Ce after a short pulse excitation at 4.9 and 3.6 eV is shown in **Figure 2**. The decay at delays longer than  $\approx 30$  ns proceeds at approximately the same rate at both excitation photon energies, while the contribution of the fast decay component is considerably more pronounced at 3.6 eV excitation. The initial part of the PL response to short-pulse excitation for both GAGG:Ce and GAGG:Ce,Mg (samples A1 and A2) is presented in **Figure 2**. The instrumental response function is also depicted there. Due to the presence of long PL decay components, the FWHM of the instrumental function was 100 ps in these experiments. For clarity, only the fits to the experimental decay data are presented in **Figure 2**. The fit is illustrated in the inset of **Figure 2**. The major part of the GAGG:Ce luminescence grows instantaneously within the experimental response time, however, a slower rise component is also observed. Thus, the PL response was fitted as  $f(t) = [A_1 + A_2 \exp(-t/\tau_r)] \exp(-t/\tau_d)$ , where  $A_1$  and  $A_2$  are amplitudes of the fast and slow growth components, while  $\tau_r$  and  $\tau_d$  are the luminescence growth and decay times. This fluorescence profile was further convoluted with the experimentally obtained response function. At the excitation of  $\text{Ce}^{3+}$  luminescence through the matrix (at 4.9 eV), the time constant of the slow rise  $\tau_r = 8$  ns. At 3.6 eV, corresponding to the resonant excitation to absorption band of  $\text{Ce}^{3+}$  ions, the time constant of the slow rise component  $\tau_r = 2.5$  ns is shorter but still considerably longer than the instrumental response function. As reported before,<sup>[13]</sup>

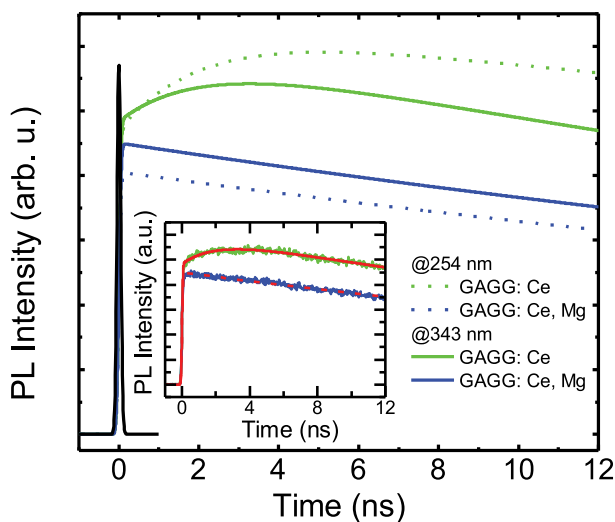


**Figure 2.** The initial part of PL response to a short excitation pulse at 343 nm of GAGG:Ce, sample A1 (green) and Mg codoped sample A2 (blue). Instrumental response function is also presented.

the slow rise component disappears in GAGG:Ce,Mg, and luminescence rise proceeds in subpicosecond time range.

Mg-codoping also influences the luminescence kinetics. Scintillation kinetics with characteristic time constants of 60 and 54 ns are observed in GAGG:Ce at 254 and 343 nm excitation, respectively. The difference between the time constants disappears in the Mg-codoped crystal; for both excitation wavelengths was found to be 51 ns.

Free carrier absorption in GAGG:Ce with and without Mg-codoping was studied in pump and probe configuration. The difference between the absorption after excitation by a short pulse (pulse energy  $0.48 \text{ mJ cm}^{-2}$ ) at 4.9 eV and the absorption without excitation was probed as a function of delay between pump and probe pulses at different probe wavelengths: 905 nm (1.38 eV), 1041 nm (1.2 eV), 1213 nm (1.03 eV), 1404 nm (0.89 eV), and 1712 nm (0.73 eV) both for GAGG:Ce (sample A1) and GAGG:Ce,Mg (A2). The decay of the normalized differential absorption signals of probing radiation at three typical probe wavelengths are presented in **Figure 3**.

For the probe photon energy down to  $\approx 1$  eV, the decay kinetics exhibit minor dependence on the probe photon energy. Both for GAGG:Ce and GAGG:Ce,Mg, the decay consists of a fast decay component and the decay proceeding at a slower rate, with the decay time of 40–50 ns for both crystals. The fast decay component is considerably more pronounced in GAGG:Ce, Mg. For probe photon energy of below 1 eV, the slow decay component becomes faster in GAGG:Ce, while the fast decay component becomes more pronounced in both crystals.

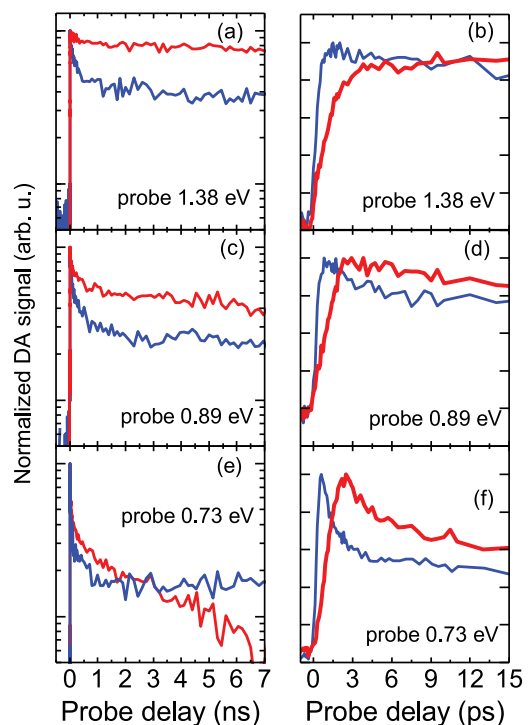


**Figure 3.** Normalized differential absorption signals at different probe photon energies (indicated) in nano- (left panel) and picosecond (right panel) domains of GAGG:Ce (red) and GAGG:Ce,Mg (blue).

As reported before,<sup>[13]</sup> the rise edge in the DA response of GAGG:Ce consists of two components: the first one is faster than the excitation pulse rise time (in subpicosecond domain), and the second is slower, on the order of a few picoseconds. In this paper, we show that decreasing the probe photon energy down to  $\approx 1$  eV does not have a substantial influence on the DA rise edge. Meanwhile, the slow rise component for the probe photon energy above  $\approx 1$  eV becomes more pronounced.

The dependence of the DA peak value on the probe photon energy is presented in **Figure 4**. The dependence does not follow the typical FCA spectrum but rather has distinct features, which are probably caused by absorption to specific energy levels.

### 3.2. Probing the Trapping Centers in GAGG:Ce Crystals by Thermally Stimulated Luminescence Technique

The trapping levels in GAGG with different structural defects were studied using the thermally stimulated luminescence (TSL) techniques in the set of three samples (B1–B3) grown with different deviations from crystal stoichiometry. This study was focused on revealing the crystal defects which come from the intrinsic properties of the material and are not influenced by technological conditions.

First of all, the defects caused by preferential evaporation of the most volatile component from the melt during crystal growth are expected. The formation of such defects has been clearly observed in the growth of single crystals in the binary systems  $\text{PbO-WO}_3$  and  $\text{Al}_2\text{O}_3\text{-Y}_2\text{O}_3$ .<sup>[29]</sup> In the  $\text{Gd}_2\text{O}_3\text{-Al}_2\text{O}_3\text{-Ga}_2\text{O}_3$  system, gallium oxide is the most volatile compound<sup>[30]</sup> and evaporates faster than other constituents in the melted raw material. The structure of the garnet-type crystals under study belongs to the cubic space group  $Ia\bar{3}d$  (#230) with the cations in spatial positions (on  $16a$ ,  $24c$ , and  $24d$  sites) and oxygen anions in the general positions (on  $96h$  sites).<sup>[31]</sup> Three cations have tetrahedral coordination ( $24d$  sites) and two cations have octahedral ( $16a$  sites) coordination formed by oxygen ions.

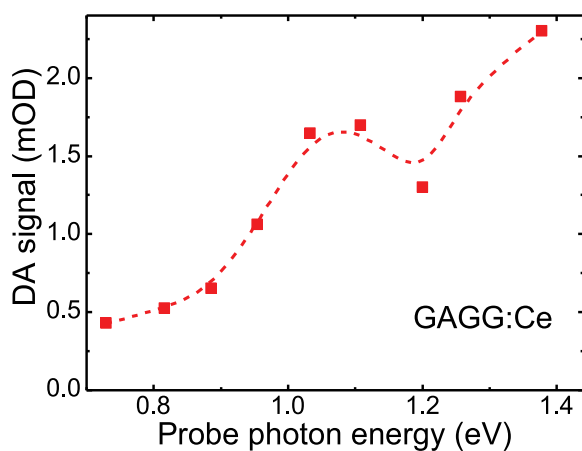


**Figure 4.** Peak differential absorption of GAGG:Ce as a function of probe photon energy.

The eighth coordinate sites (dodecahedral,  $24c$  sites) accommodate rare earth ion or yttrium. In a disordered GAGG crystal, 60% of  $\text{Ga}^{3+}$  ions occupy the tetrahedral sites, whereas 40% octahedral sites. The formation of cation vacancies due to the gallium evaporation inevitably leads to the formation of anionic vacancies in octahedrons and tetrahedrons and, as a consequence, of trapping centers based on such vacancies.

The use of the Al–Ga mixture to make crystal introduces two side effects: i) site occupancy disorder and ii) formation of additional defects that act as trapping centers for nonequilibrium carriers. The ratio of the ionic radii of Al and Ga is 0.83 and 0.85 in the oxygen tetrahedral and octahedral positions.<sup>[32]</sup> Therefore, even a random distribution of Al and Ga ions in the lattice results in considerable distortion of the lattice. Due to this reason the multicomponent gadolinium garnets containing gallium and aluminum should contain more structural defects than the binary garnet crystals do. Moreover, gallium and aluminum ions located in close proximity also result in considerable lattice strain, lead to distortion of the polyhedra, and, as a consequence, result in formation of numerous characteristic shallow trapping centers. The samples without codoping exhibit room temperature phosphorescence at photoexcitation in the absorption bands of both  $\text{Ce}^{3+}$  and  $\text{Gd}^{3+}$ . Worth to note, the spectra of the TSL glow creation, absorption spectra of  $\text{Ce}^{3+}$  ions and spectra of phosphorescence creation coincide.<sup>[33]</sup>

**Figure 5** shows the TSL curves and the thermal activation energy  $E_{\text{TA}}$  of the traps corresponding to the glow peaks measured in the samples B1–B3. Similar to the data presented in Refs. [17,34,35], strong TSL peaks of complex structure have been detected in GAGG crystal in the temperature range 25–100 K. In TSL of all the samples,  $\text{Ce}^{3+}$  luminescence is observed and the TSL spectra also exhibit a glow peak above RT near 395 K, as reported in Ref. [33]. The shallow traps are better resolved in sample B1 (with stoichiometric melt composition) than in samples B2 and B3 (nonstoichiometric). We observed that the amount of the groups of the shallow traps having  $E_{\text{TA}}$  within the range 0.02–0.2 eV does not change drastically from sample to sample. However, the intensities of the corresponding TSL peaks are affected by the addition of excess Ga and Zr-codoping.

The comparison of TSL spectra in samples B1–B3 shows that the introduction of excess Ga increases the intensity of the TSL bands in the range 150–300 K. On the contrary, the codoping with  $\text{Zr}^{4+}$  reduces the intensity of the TSL bands in this temperature range but gives the rise to the band above 350 K. However, both additional Ga or Zr ions do not change significantly the group of TSL peaks below 150 K. Thus, we suggest that shallow traps with  $E_{\text{TA}}$  smaller than 0.1 eV most probably are caused by distortions of the polyhedra, as it was noted above, whereas the traps with larger  $E_{\text{TA}}$  correspond to structural point defects, most probably anion vacancies, the concentration of which is affected by applied codopings. It is worth noting that the activation energies of the deepest traps we observe by applying the TSL technique to the samples under study are smaller than  $\approx 0.2$  eV. This is consistent with the results presented in Ref. [36], where the deepest trapping levels are reported at  $\approx 0.3$  eV below the bottom of the conduction band.

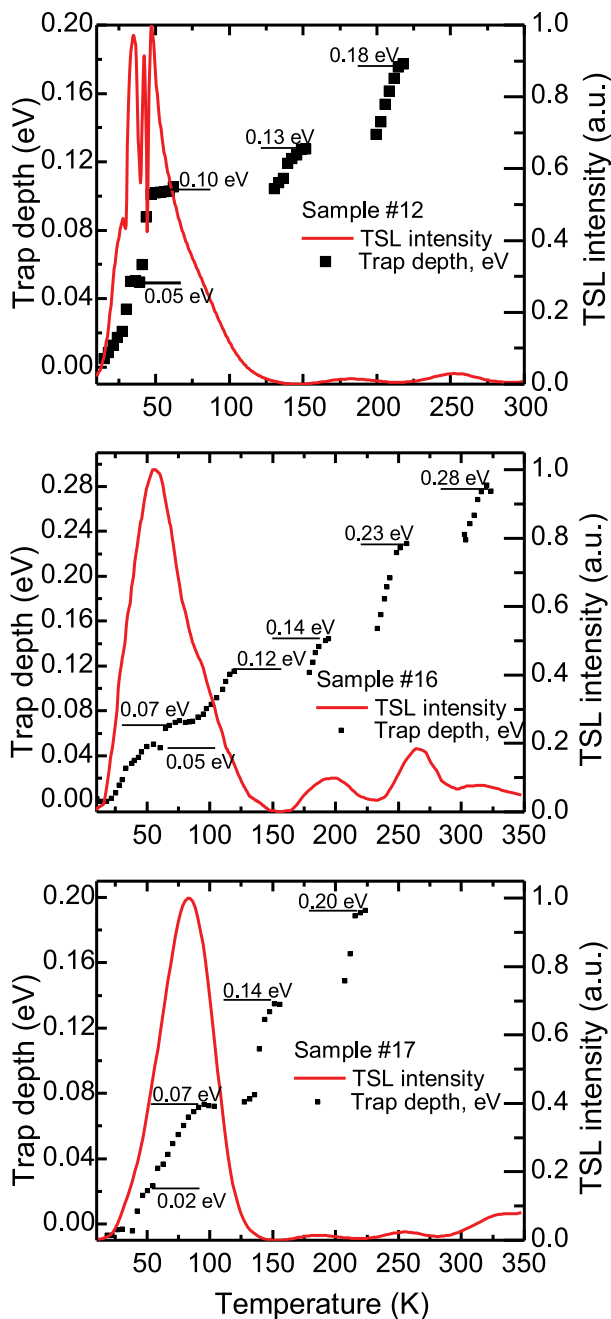


**Figure 5.** TSL curve (red) and  $E_{TA}$  of the traps (points) observed in samples B1, B2, and B3 (from top to bottom).

### 3.3. Luminescence Build Up in LSO:Ce Crystals

The excitation transfer in GAGG is strongly influenced by  $Gd^{3+}$ . The transfer is expected to be simpler in oxyorthosilicate crystal  $Lu_2SiO_5$  (LSO). Similarly to GAGG, aliovalent codoping introduces an additional absorption band in UV range. To reveal the general features of the codoping effect, we compared the differential absorption spectra of solely doped with Ce and codoped with  $Ca^{2+}$  crystals of  $Lu_2SiO_5$  (L1) and isostructural  $Y_2SiO_5$  (L2), see **Figure 6**. In oxyorthosilicate structure, calcium

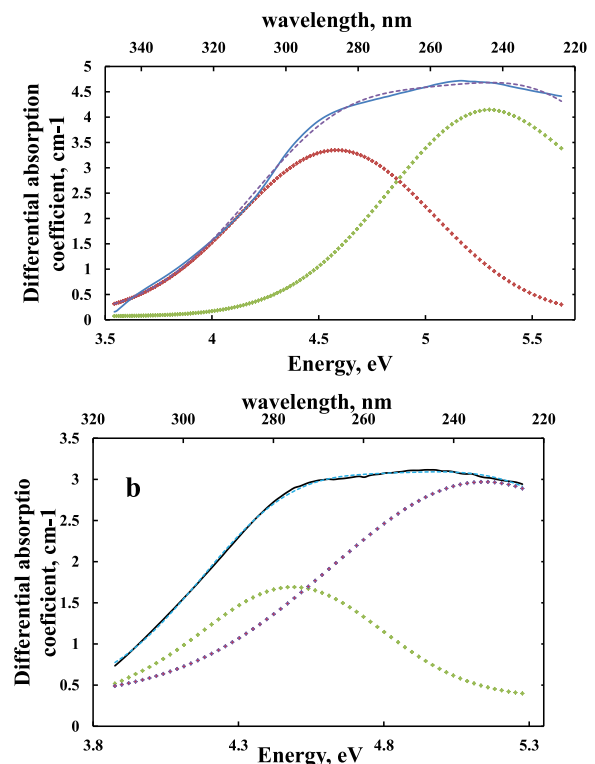


**Figure 6.** Spectra of difference in absorption coefficients with and without calcium codoping in LSO:Ce (a) and YSO:Ce (b). The dashed line represents the best fit by two Gaussian-shaped components (dotted lines).

ions substitute lutetium ions, which have two inequivalent positions with six and seven oxygen neighbors. The introduction of divalent ions into the oxyorthosilicate single crystal results in a broad absorption band consisting of two strongly overlapping bands. The calcium-induced absorption spectrum can be well fitted by two Gaussian-shaped bands (dotted lines in **Figure 6**; Pearson's chi-square test value  $\chi^2 = 4 \times 10^{-3}$  for LSO:Ce and  $10^{-3}$  for LYSO:Ce). The two components have peaks at 270 and 235 nm in LSO:Ce and 275 and 240 nm in YSO:Ce. The two bands in the absorption spectrum of oxyorthosilicates are consistent with two possible  $Ca^{2+}$  ion positions of localization in the host matrix, 6(O) and 7(O), instead of a single position 8(O) in scintillators with a garnet structure. Obviously, a similar two-component absorption band should be formed in mixed crystal LYSO.

To get information on excitation transfer in LSO:Ce (a) and YSO:Ce, the nonlinear optical absorption induced by a short pulse of UV photons was studied. 200-fs-long pulses at 4.9 eV (254 nm) were used for excitation. The excitation photon energy is lower than the band gap of both LSO (6.4 eV) and YSO but is sufficient to excite cerium ions into the first and second excited state. The spectrum of the transient differential absorption (DA) of LSO:Ce (sample L3) contains one wide band overlapping the range 460–730 nm and peaked at 580 nm.

The initial part of the kinetics of the spectrally integrated DA signal is presented in **Figure 7**. The signal appears simultaneously with the leading edge of the pump pulse. The decay of the DA proceeds on a nanosecond time scale (see inset in

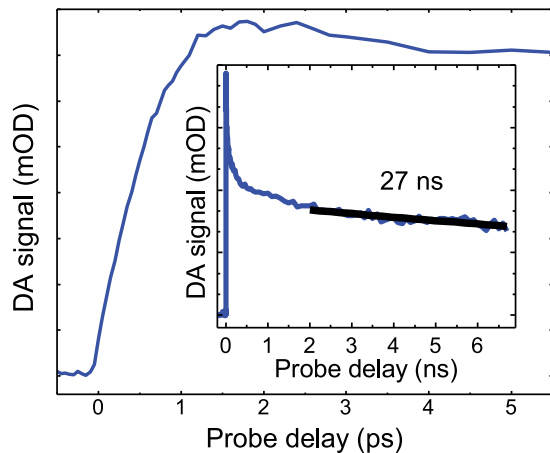


**Figure 7.** Kinetics of differential absorption in LSO:Ce, sample L3, in picosecond and nanosecond (inset) domains probed at 650 nm after 200-fs-pulse excitation at 254 nm.

Figure 7) and has two components. The fast component has the time constant of  $\approx 200$  ps and its time-integrated weight is small in comparison with that of the slow component decaying with the time constant of  $\approx 27$  ns. This time constant is close to the decay time of excitation at  $\text{Ce}^{3+}$  radiating level. This is an indication that the observed transient absorption is predominantly caused by electrons populating the  $\text{Ce}^{3+}$  radiating level. The fast decay component of the differential absorption can be reasonably explained by capturing of the photoexcited electrons from  $\text{Ce}^{3+}$  excited state by traps. The small relative weight of this component indicates low concentration of the trapping centers and, consequently, high structural perfection of the crystal.

## 4. Discussion

### 4.1. Excitation Transfer in GAGG:Ce and GAGG:Ce,Mg Crystals

The photon energy of 3.6 eV (343 nm) is well below the band gap of GAGG. Thus, such photons predominantly excite  $\text{Ce}^{3+}$  ions in GAGG crystal. Nevertheless, GAGG:Ce at such photoexcitation exhibits strong phosphorescence,<sup>[37]</sup> which could be explained by the transfer of photoexcited electrons from the first excited state of  $\text{Ce}^{3+}$  to the conduction band, their trapping at shallow defect-related levels, thermally induced detrapping and return back to  $\text{Ce}^{3+}$  ions to recombine radiatively and cause the phosphorescence. For the efficient transfer of photoexcited electrons from  $\text{Ce}^{3+}$  ions to the conduction band, the first Stark component of the  $5d^1f^0$  configuration  $\text{Ce}^{3+}$  should be close to the bottom of the conduction band.

The photon energy of 4.9 eV (254 nm), which was also used for excitation in our experiments, is sufficient to excite not only  $\text{Ce}^{3+}$  ions, as at 3.6 eV excitation, but also  $\text{Gd}^{3+}$  ions via the  $^8\text{S} \rightarrow ^6\text{D}_{7/2,9/2}$  transitions. Thus, the photons with energy of 4.9 eV generate free electrons via absorption by  $\text{Ce}^{3+}$  and subsequent transfer of the electrons to the conduction band and free holes via excitation of gadolinium ions. The concentration of  $\text{Ce}^{3+}$  ions at the doping level of 0.5 at.% is substantially lower than the

concentration of crystal-building Gd ions, therefore, the density of free electrons at this excitation is considerably smaller than that of free holes, in contrast to the excitation at 3.6 eV generating no free holes. As pointed out in our previous paper,<sup>[38]</sup> the PL kinetics is consistent with the assumption that the ground  $^8\text{S}$  level of  $\text{Gd}^{3+}$  is in the valence band. The current results on the differential absorption (see Figure 4) enables us to define the position of the  $\text{Gd}^{3+}$  ground state in the valence band. The differential absorption caused by free holes in the valence band should have a smooth proportionality of the absorption coefficient on the wavelength squared. Instead, we observe a structured increase with the photon energy. This dependence should be explained by the influence of the resonant energy levels in the valence band. Thus, the hump in the DA spectrum peaked at 1.05 eV has to be attributed to the position of the Gd ground state, i.e., the state is  $\approx 1$  eV below the top of the valence band.

Furthermore, the excitations at 3.6 and 4.9 eV enables us to study the transfer of nonequilibrium electrons and holes, respectively, by comparing the PL kinetics of GAGG:Ce. The PL rise time in GAGG:Ce after direct excitation of  $\text{Ce}^{3+}$  at 3.64 eV is 2 ns. As suggested in Ref. [38], this substantial delay in reaching the peak PL intensity is caused by the time necessary for establishing the equilibrium between trapping and detrapping of the free electrons, which are released into the conduction band from the  $\text{Ce}^{3+}$  excited level. The PL rise time after the predominant  $\text{Gd}^{3+}$  excitation at 4.9 eV is by a factor of three longer than that after the direct excitation. Thus, the excitation transfer from the gadolinium sublattice to the radiative  $\text{Ce}^{3+}$  sites takes a few nanoseconds, what is caused by a relatively slow migration of excitations along the Gd sublattice.<sup>[39]</sup>

The presence of a distinct absorption band in the instantaneous DA spectrum correlates with the qualitative transformation of the DA kinetics (see Figure 3). The DA signal rises with characteristic time constant of 1.5 ps. The rise exhibits no significant dependence on the probe energy and, most probably, is predominantly determined by the relaxation of holes from the  $\text{Gd}^{3+}$  ground level toward the top of the valence band. The decay kinetics shows that the DA has two decay components. The response is dominated by a component with the characteristic decay time of 40–50 ns. In addition, a fast decaying component is observed at the initial part of the DA decay. The fast component might be attributed to absorption by free electrons. The time-integrated contribution of this component is approximately by three orders of magnitude smaller than that of the slow component caused by free hole absorption. Note that the fast component is more pronounced for the probe photon energy below  $\approx 1$  eV. At larger probe photon energies, when the free hole absorption is enhanced due to the optical transitions of free holes to the ground state of Gd ions, the relative contribution of the fast component becomes less pronounced.

The rising part in the DA response of the Mg-codoped crystal becomes considerably faster (see Figure 3) due to contribution of  $\text{Mg}^{2+}$ -based defect centers in the generation of free holes at the top of valence band by absorbing 4.9 eV pump light. The defect centers cause additional nonradiative recombination. As a result, the DA signal decay is faster in the codoped crystal.

Thus, the slow rise component with characteristic time of a few nanoseconds in the GAGG:Ce luminescence response after

short-pulse excitation is caused by trapping and detrapping of nonequilibrium electrons. In Mg-codoped crystals, the trapped electrons predominantly relax to the energy levels introduced by Mg-doping and recombine nonradiatively or are transferred to  $\text{Ce}^{3+}$ . As a result, the luminescence response to a short-pulse excitation becomes shorter, but the light yield decreases.

To clarify the energy transfer processes in GAGG, we sketched a simple energy level diagram of all the main structural units involved in the excitation transfer process (see **Figure 8a**). This diagram does not include configuration potential curves for d-type states, which are usually considered for the transitions with a large Stokes shift. For simplicity, we considered just the positions of zero-phonon states of the Stark components of d-states. The energy diagrams in Gd-based crystals have been discussed in Refs. [40–42]. The energy-level diagram for  $\text{Ce}^{3+}$  in GAGG has been already described in Ref. [43], where the band gap of 6.8 eV was used. Different band gap values are also reported in Ref. [44]. The energy differences between  $\text{Ce}^{3+}$  levels used in this paper are based on the positions of the absorption and luminescence bands reported in Ref. [38]. Taking into account that the lowest zero-phonon radiating level of  $\text{Ce}^{3+}$  is located by 0.3 eV below the bottom of the conduction band,<sup>[33]</sup> we conclude that the center of gravity of the  $f^1$ -state is 2.6 eV below the radiating level. Thus, the  $f^1$ -level is  $\approx 3.35$  eV above the top of the valence band.

Our DA study described above shows that the position of the gadolinium  $^8\text{S}$  level is by  $\approx 1$  eV lower than the top of the valence band. The position of the lowest terms corresponding to the excited states of  $f^7$   $\text{Gd}^{3+}$  was estimated using absorption spectra (see, e.g., Ref. [38]). The corresponding positions of narrow P, I, and D states without accounting for their splitting by spin-orbit interaction are indicated in the diagram. These energy positions favor the excitation transfer from the  $\text{Gd}^{3+}$  sublattice to  $\text{Ce}^{3+}$  ions. The efficiency of this transfer is evidenced by strong luminescence at  $\text{Ce}^{3+}$  ions even after the predominantly resonant excitation of gadolinium sublattice at excitation with 4.9 eV photons.

The band gap of GAGG contains defect-related states. As evidenced by the TSL study presented above, intrinsic structural defects impose the states, which are located below the band gap not deeper than  $\approx 0.3$  eV. These levels trap electrons from the conduction band, while the thermal reexcitation of the electrons back to the conduction band results in delayed luminescence.

Our results show that the defect related with  $\text{Mg}^{2+}$  in GAGG has a broad absorption band, most probably due to a charge transfer transition. Therefore, the corresponding energy level in the band gap of GAGG is well below the trapping states but higher than the P, I, and D states of  $\text{Gd}^{3+}$ . As seen in the diagram, Gd- and Ce-related transitions and traps have poor resonance conditions. Thus, the probability of tunneling from traps to Gd subsystem is low, a considerable fraction of the trapped electrons are detrapped and take part in phosphorescence. The defects introduced by codoping with Mg might capture the electrons trapped at shallow centers. This capture is evidenced by the substantial decrease in intensity of the TSL bands due to relatively shallow traps, as discussed above, and is consistent with the results presented in Refs. [34,36]. The electrons captured down to Mg-related defects might follow two possible roots: i) be transferred to  $\text{Gd}^{3+}$  states and further to  $\text{Ce}^{3+}$  or ii) recombine nonradiatively at the defect with the free hole from the valence band. The first root results in a faster rise of luminescence response after short-pulse excitation and diminishes the delayed luminescence. Meanwhile, the additional channel of nonradiative recombination, which is introduced by Mg-codoping, reduces the light yield of GAGG:Ce.

The results discussed above show that the nonequilibrium holes reach the radiative  $\text{Ce}^{3+}$  centers faster than the nonequilibrium electrons do. This is an indication that, at a relatively small concentration of Mg ions, as in the samples studied in the current paper, the scintillation mechanism due to the consecutive capturing of the carriers, holes and electrons, by  $\text{Ce}^{3+}$  ions is still dominating.

The competition of hole capturing by  $\text{Ce}^{3+}$  ion and its nonradiative recombination at  $\text{Mg}^{2+}$ -based defect explains the

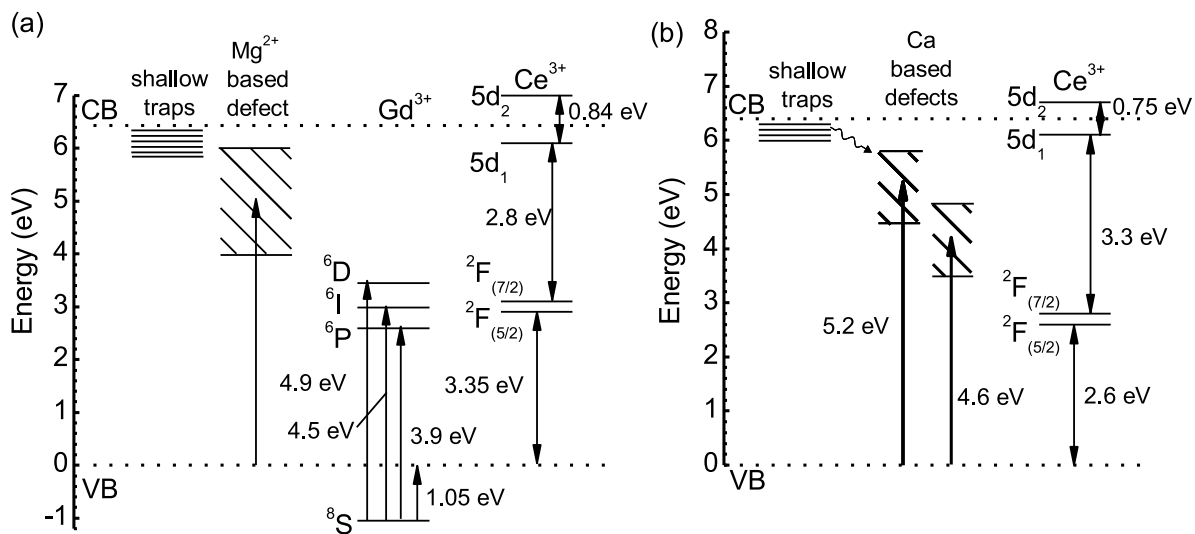


**Figure 8.** Energy-level diagram for GAGG crystal doped with Ce and codoped with Mg (a) and for LSO doped with Ce and codoped with Ca (b).



improvement of the light yield of codoped GAGG samples with temperature decrease, as described in Ref. [16], where it is shown by the gated light yield measurements that the scintillation kinetics is not changed in the temperature range from room temperature down to  $-45^{\circ}\text{C}$ , while the light yield increases by 20%. An increase of the light yield with a minor temperature decrease below room temperature is not typical for Ce-doped scintillation crystals.<sup>[29]</sup> Most probably, the observed gain in the light yield at lower temperatures is the result of increased lifetime of holes. The carrier recombination, which is in our case a Shockley–Read–Hall process,<sup>[45–47]</sup> is temperature dependent. The carrier lifetime depends on the capture rate, which decreases as temperature is decreased. A possible mechanism of the decrease is longer time the holes remain at the  $^8\text{S}$  level of  $\text{Gd}^{3+}$ , which is below the top of the valence band.

#### 4.2. Excitation Transfer in Oxyorthosilicates

In crystals containing no matrix-building  $\text{Gd}^{3+}$  ions, the resonance conditions between  $\text{Ce}^{3+}$  and Ca (Mg) related defect play the crucial role. The crystal field at the  $\text{Ce}^{3+}$  ion positions is smaller in LSO, YSO, and LYSO than that is GAGG. Therefore, the energy difference between  $^2\text{F}$  states and the first Stark component of  $4f^95d^1$  configuration is larger. The energy level diagram for LSO, like that described above for GAGG:Ce, is presented in Figure 8b. Similar diagrams are also expected for YSO and LYSO crystals. The main difference between LSO and GAGG is a faster electron transfer due to a better overlapping between the broad subbands due to the defects associated with divalent ion and the interconfiguration absorption bands of the radiative Ce centers.

In contrary to GAGG, where shallow defects dominate, LSO have trapping centers with large activation energy resulting in TSL peaks at 354, 410, 462, 524, and 569 K, which are related to oxygen vacancies.<sup>[48,49]</sup> Similar to GAGG:Ce, codoping with divalent ions facilitates the electron transfer from the traps to  $\text{Ce}^{3+}$ .

The codoping of oxyorthosilicates by divalent ions improves both the time characteristics of luminescence response and the light yield of the crystal. In contrary to GAGG, LSO has no peculiarities in the valence zone. Thus, hole dynamics in LSO and nonradiative recombination at the Ca-based centers are less sensitive to the temperature change. As a result, the luminescence build-up process is practically the same in LSO with and without codoping. This is also proven by gated light yield measurements showing that the light yield is insensitive to temperature down to  $-45^{\circ}\text{C}$ .<sup>[50]</sup>

The results discussed above allow making suggestions on the choice of the optimal oxide compound in view of both improvement of timing characteristics and a high light yield. First, the compound should have crystal field for Ce stabilization similar or larger than in orthosilicates in order to balance resonance transfer conditions from alkali-earth-based defect to activator. The choice of the crystal matrix with smaller crystal field at the  $\text{Ce}^{3+}$  position results in a decrease of the scintillation light yield, as in  $\text{YAlO}_3$  codoped with Ce and Ca.<sup>[51]</sup> As already published, the defects practically do not affect the photoluminescence decay time, but strongly

reduce the decay time of scintillation and the light yield. This is an evidence of weak quenching of  $\text{Ce}^{3+}$  luminescence by Ca-based defects and strong competition of the defects and  $\text{Ce}^{3+}$  ions in receiving excitation from matrix. Similar effect is observed when crystal is doped with  $\text{Pr}^{3+}$  and codoped with alkali-earth ions.<sup>[52]</sup> The inter-configuration  $4f5d \rightarrow f^2$  luminescence of  $\text{Pr}^{3+}$  consists of two overlapped wide unstructured bands at room temperature, usually in the UV range. Large energy of the emitting state does not allow an effective transfer from alkali-earth-based defect.

## 5. Conclusion

Our time-resolved study of the photoluminescence response to short-pulse excitation at different wavelengths and free carrier absorption, supported by the results available in the literature, enabled us to explain the changes of the scintillation parameters of GAGG:Ce and LSO:Ce imposed by additional aliovalent codoping.

It is shown that the ground state of lattice-building gadolinium ions in GAGG crystal is in the valence band by  $\approx 1$  eV from its top. The gadolinium sublattice plays a significant role in the transfer of both nonequilibrium holes and electrons. As a result, the luminescence response to a short-pulse excitation becomes shorter, but the light yield decreases.

In Ce-doped oxyorthosilicates, the overlap between i) the electron trap levels; ii) a broad subband due to defects related with divalent ion; and iii) the excited level of radiative  $\text{Ce}^{3+}$  ions is better than that in GAGG:Ce,Mg, thus, codoping with divalent ions results in improvement of both time response and light yield.

## Acknowledgments

This work has been supported by the European Social Fund Measure No. 09.3.3-LMT-K-712 activity Improvement of Researchers Qualification by Implementing the World-Class R&D Projects, and by grant #14.W03.31.0004 of the Russian Federation Government. Authors are grateful to CERN Crystal Clear Collaboration and COST Action TD1401 “Fast Advanced Scintillator Timing (FAST)” for support of collaboration.

## Conflict of Interest

The authors declare no conflict of interest.

## Keywords

excitation transfer, free carriers, multicomponent garnets, scintillators

Received: October 20, 2017

Revised: January 25, 2018

Published online:

[1] K. Kamada, T. Endo, K. Tsutumi, T. Yanagida, Y. Fujimoto, A. Fukabori, A. Yoshikawa, J. Pejchal, M. Nikl, *Cryst. Growth Des.* **2011**, *3*, 4484.

- [2] K. Kamada, T. Yanagida, J. Pejchal, M. Nikl, T. Endo, K. Tsutsumi, Y. Fujimoto, A. Fukabori, A. Yoshikawa, *IEEE Trans. Nucl. Sci.* **2012**, 59, 2112.
- [3] S. K. Yadav, B. P. Uberuaga, M. Nikl, C. Jiang, C. R. Stanek, *Phys. Rev. Appl.* **2015**, 4, 1.
- [4] M. Fasoli, A. Vedda, M. Nikl, C. Jiang, B. P. Uberuaga, D. A. Andersson, K. J. McClellan, C. R. Stanek, *Phys. Rev. B – Condens. Matter Mater. Phys.* **2011**, 84, 1.
- [5] H. L. Kim, H. J. Kim, E. J. Jang, W. G. Lee, M. K. Ki, H. D. Kim, G. S. Jun, V. Kochurikhin, *J. Ceram. Process. Res.* **2015**, 16, 124.
- [6] E. V. D. van Loef, P. Dorenbos, C. W. E. van Eijk, K. Krämer, H. U. Güdel, *Appl. Phys. Lett.* **2001**, 79, 1573.
- [7] N. J. Cherepy, S. A. Payne, S. J. Asztalos, G. Hull, J. D. Kuntz, T. Niedermayr, S. Pimputkar, J. J. Roberts, R. D. Sanner, T. M. Tillotson, E. Van Loef, C. M. Wilson, K. S. Shah, U. N. Roy, R. Hawrami, A. Burger, L. A. Boatner, W. S. Choong, W. W. Moses, *IEEE Trans. Nucl. Sci.* **2009**, 56, 873.
- [8] Z. Yan, T. Shalapska, E. D. Bourret, *J. Cryst. Growth* **2016**, 435, 42.
- [9] K. Kamada, M. Nikl, S. Kurosawa, A. Beitlerova, A. Nagura, Y. Shoji, J. Pejchal, Y. Ohashi, Y. Yokota, A. Yoshikawa, *Opt. Mater. (Amst)*. **2015**, 41, 63.
- [10] G. Dosovitskiy, A. Fedorov, V. Mechinsky, A. Borisevich, A. Dosovitskiy, E. Tret'jak, M. Korjik, *IOP Conf. Series: Mater. Sci. Eng.* **2017**, 169, 012014.
- [11] M. A. Spurrier, P. Szupryczynski, K. Yang, A. A. Carey, C. L. Melcher, *IEEE Trans. Nucl. Sci.* **2008**, 55, 1178.
- [12] S. Blahuta, A. Bessiere, B. Viana, P. Dorenbos, V. Ouspenski, *IEEE Trans. Nucl. Sci.* **2013**, 60, 3134.
- [13] G. Tamulaitis, A. Vaitkevičius, S. Nargelas, R. Augulis, V. Gulbinas, P. Bohacek, M. Nikl, A. Borisevich, A. Fedorov, M. Korjik, E. Auffray, *Nucl. Instruments Methods Phys. A* **2017**, 870, 25.
- [14] M. T. Lucchini, V. Babin, P. Bohacek, S. Gundacker, K. Kamada, M. Nikl, A. Petrosyan, A. Yoshikawa, E. Auffray, *Nucl. Instruments Methods Phys. A* **2016**, 816, 176.
- [15] M. T. Lucchini, S. Gundacker, P. Lecoq, A. Benaglia, M. Nikl, K. Kamada, A. Yoshikawa, E. Auffray, *Nucl. Instruments Methods Phys. A* **2017**, 852, 1.
- [16] M. Korjik, V. Alenkov, A. Borisevich, O. Buzanov, V. Dormenev, G. Dosovitskiy, A. Dosovitskiy, A. Fedorov, D. Kozlov, V. Mechinsky, R. W. Novotny, G. Tamulaitis, V. Vasiliev, H-G Zaunick, A. Vaitkevičius, *Nucl. Instruments Methods Phys. A* **2017**, 871, 42.
- [17] W. Drozdowski, K. Brylew, M. E. Witkowski, A. J. Wojtowicz, P. Solarz, K. Kamada, A. Yoshikawa, *Opt. Mater. (Amst)*. **2014**, 36, 1665.
- [18] M. Nikl, V. Babin, J. Pejchal, V. V. Laguta, M. Buryi, J. A. Mares, K. Kamada, S. Kurosawa, A. Yoshikawa, D. Panek, T. Parkman, P. Bruza, K. Mann, M. Müller, M. Muller, *IEEE Trans. Nucl. Sci.* **2016**, 63, 433.
- [19] C. Hu, S. Liu, M. Fasoli, A. Vedda, M. Nikl, X. Feng, Y. Pan, *Opt. Mater. (Amst)*. **2015**, 45, 252.
- [20] Y. Wu, F. Meng, Q. Li, M. Koschan, C. L. Melcher, *Phys. Rev. Appl.* **2014**, 2, 1.
- [21] M. Nikl, K. Kamada, V. Babin, J. Pejchal, K. Pilarova, E. Mihokova, A. Beitlerova, K. Bartosiewicz, S. Kurosawa, A. Yoshikawa, *Cryst. Growth Des.* **2014**, 14, 4827.
- [22] M. Spurrier, P. Szupryczanski, A. carey, K. Yang, C. Melcher, *IEEE Trans. Nucl. Sci.* **2008**, 55, 1178.
- [23] M. Koschan, K. Yang, M. Zhuravleva, C. L. Melcher, *J. Cryst. Growth* **2012**, 352, 133.
- [24] M. S. Alekhin, J. T. M. De Haas, I. V. Khodyuk, K. W. Krämer, P. R. Menge, V. Ouspenski, P. Dorenbos, *Appl. Phys. Lett.* **2013**, 102, 1.
- [25] F. G. A. Quarati, M. S. Alekhin, K. W. Krämer, P. Dorenbos, *Nucl. Instruments Methods Phys. Res. Sect. A Accel. Spectrometers, Detect. Assoc. Equip.* **2014**, 735, 655.
- [26] K. Yang, P. Menge, J. Frank, Scintillation crystal including a co-doped sodium halide, and a radiation detection apparatus including the scintillation crystal, International Patent Application PCT/US2016/017945.
- [27] K. Yang, C. L. Melcher, P. D. Rack, L. A. Eriksson, *IEEE Trans. Nucl. Sci.* **2009**, 56, 2960.
- [28] R. Chen, V. Pagonis, *Thermally and Optically Stimulated Luminescence: A Simulation Approach*. John Wiley & Sons, USA **2011**, pp. 434.
- [29] P. Lecoq, A. Gektin, M. Korzhik, Springer, Germany **2017**, p. 408.
- [30] R. H. Lamoreaux, D. L. Hildenbrand, L. Brewer, *J. Phys. Chem. Ref. Data* **1987**, 16, 419.
- [31] A. Nakatsuka, A. Yoshiasa, T. Yamanaka, *Acta Crystallogr. Sect. B.* **1999**, 55, 266.
- [32] R. D. Shannon, *Acta Crystallogr. Sect. A* **1976**, 32, 751.
- [33] E. Auffray, R. Augulis, A. Borisevich, V. Gulbinas, A. Fedorov, M. Korjik, M. T. Lucchini, V. Mechinsky, S. Nargelas, E. Songaila, G. Tamulaitis, A. Vaitkevičius, S. Zazubovich, *J. Lumin.* **2016**, 178, 54.
- [34] E. Mihóková, K. Vávrů, K. Kamada, V. Babin, A. Yoshikawa, M. Nikl, K. Vávr, K. Kamada, V. Babin, A. Yoshikawa, M. Nikl, *Radiat. Meas.* **2013**, 56, 98.
- [35] K. Brylew, W. Drozdowski, A. J. Wojtowicz, K. Kamada, A. Yoshikawa, *J. Lumin.* **2014**, 154, 452.
- [36] K. Mamoru, K. Kei, K. Shunsuke, A. Junpei, O. Akimasa, Y. Akihiro, H. Kazuhiko, *Appl. Phys. Express* **2016**, 9, 72602.
- [37] G. Dosovitskiy, O. Buzanov, A. Dosovitskiy, A. Fedorov, L. Grigorjeva, M. Korjik, V. Mechinsky, S. Nargelas, G. Tamulaitis, V. Vasiliev, S. Zazubovich, A. Zolotarjovs, Gd<sub>3</sub>Al<sub>2</sub>Ga<sub>3</sub>O<sub>12</sub>:Ce stoichiometry deviation influence on the crystal scintillation properties, 19<sup>th</sup> International Conference on Defects in Insulating Materials, Abstrct, ICDIM **2016**, 10–15 July 2015, Lyon, France.
- [38] E. Auffray, M. Korjik, M. T. Lucchini, S. Nargelas, O. Sidletskiy, G. Tamulaitis, Y. Tratsiak, A. Vaitkevičius, *Opt. Mater. (Amst)*. **2016**, 58, 461.
- [39] N. V. Selina, E. N. Tumaev, *Optics and Spectroscopy* **2002**, 92, 697.
- [40] H. Suzuki, T. A. Tombrello, C. L. Melcher, C. A. Peterson, J. S. Schweitzer, *Nucl. Inst. Methods Phys. Res. A* **1994**, 346, 510.
- [41] H. Suzuki, T. A. Tombrello, C. L. Melcher, J. S. Schweitzer, 1993 *IEEE Conf. Rec. Nucl. Sci. Symp. Med. Imaging Conf.* **1994**, 41, 14.
- [42] H. Suzuki, T. A. Tombrello, C. L. Melcher, J. S. Schweitzer, *J. Lumin.* **1994**, 60–61, 960.
- [43] F. Meng, M. Koschan, Y. Wu, C. L. Melcher, P. Cohen, *Nucl. Instruments Methods Phys. Res. Sect. A Accel. Spectrometers, Detect. Assoc. Equip.* **2015**, 797, 138.
- [44] J. M. Ogieglo, Luminescence and Energy Transfer in Garnet Scintillators, Doctoral Thesis, Utrecht University, **2012**.
- [45] W. Shockey, W. T. Read, *Phys. Rev.* **1952**, 87, 387.
- [46] H. Queisser, *Solid-State Electron.* **1978**, 21, 1495.
- [47] J. Divkovic, *AUTOMATIKA* **2002**, 43, 47.
- [48] P. Dorenbos, C. W. E. van Eijk, A. J. J. Bos, C. L. Melcher, *J. Phys. Condens. Matter.* **1994**, 6, 4167.
- [49] S. Blahuta, A. Bessière, B. Viana, V. Ouspenski, E. Mattmann, J. Lejay, D. Gourier, *Materials (Basel)* **2011**, 4, 1224.
- [50] A. Vaitkevichus, Private communication, Vilnis 25 June **2017**.
- [51] F. Moretti, K. Hovhannesian, M. Derdzian, G. A. Bizarri, E. D. Bourret, A. G. Petrosyan, C. Dujardin, *ChemPhysChem* **2017**, 18, 493.
- [52] J. Peichal, M. Buryi, V. Babin, A. Beitlerova, J. Barta, L. Havlak, K. Kamada, A. Yoshikawa, V. Laguta, M. Nikl, *J. Lumin.* **2017**, 181, 277.